Article

Structure, Self-Assembly, and Dual Role of a β-Defensin-like Peptide from the Chinese Soft-Shelled Turtle Eggshell Matrix

Rajamani Lakshminarayanan, Subramanian Vivekanandan, Ramar Perumal Samy, Yajnavalka Banerjee, Emma Ooi Chi-Jin, Kay Wah Teo, Seetharama D. S. Jois, R. Manjunatha Kini, and Suresh Valiyaveettil

J. Am. Chem. Soc., **2008**, 130 (14), 4660-4668 • DOI: 10.1021/ja075659k

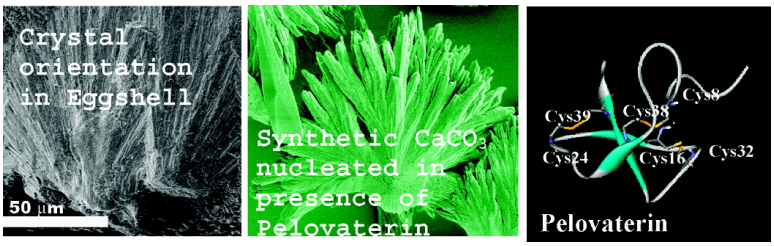

More About This Article

Additional resources and features associated with this article are available within the HTML version:

- Supporting Information
- Links to the 3 articles that cite this article, as of the time of this article download
- Access to high resolution figures
- Links to articles and content related to this article
- Copyright permission to reproduce figures and/or text from this article

View the Full Text HTML

J|A|C|S
ARTICLES
Published on Web 03/15/2008

Structure, Self-Assembly, and Dual Role of a β-Defensin-like Peptide from the Chinese Soft-Shelled Turtle Eggshell Matrix

Rajamani Lakshminarayanan,[†] Subramanian Vivekanandan,[‡] Ramar Perumal Samy,[§] Yajnavalka Banerjee,[‡] Emma Ooi Chi-Jin,[†] Kay Wah Teo,[†] Seetharama D. S. Jois,[||] R. Manjunatha Kini,[‡] and Suresh Valiyaveettil*,[†]

Department of Chemistry, Faculty of Science, 3 Science Drive 3, National University of Singapore, Singapore 117543, Protein Science Laboratory, Department of Biological Sciences, Faculty of Science, 14 Science Drive 4, National University of Singapore, Singapore 117543, Department of Anatomy, Yong Loo Lin School of Medicine, 4 Medical Drive, National University of Singapore, Singapore 117597, and Department of Basic Pharmaceutical Sciences, 700 University Avenue, University of Louisiana, Monroe, Louisiana 71209

Received July 29, 2007; E-mail: chmsv@nus.edu.sg

Abstract: Biomineral matrix formation and molecular recognition are two important processes associated with eggshell biomineralization. To understand these two processes, a major intracrystalline peptide, pelovaterin, was isolated from turtle (*Pelodiscus sinensis*) eggshell and its tertiary and quaternary structures were established. The global fold of pelovaterin is similar to that of human β-defensins but has a large hydrophobic core and a short hydrophilic N-terminal segment, which is not preserved in defensins. Pelovaterin exhibits strong antimicrobial activity against two pathogenic Gram-negative bacteria, *Pseudomonas aeruginosa* and *Proteus vulgaris*, and stabilizes a thin film of metastable vaterite. We show that pelovaterin self-aggregates in the form of micellar nanospheres and the aggregation in solution is entropy-driven. It is suggested that the micellar aggregation of pelovaterin is responsible for the induction and stabilization of the metastable phase by altering the interfacial energy. The results demonstrate the adaptability of an extracellular matrix protein to perform multiple tasks: polymorph discrimination and protection of the contents of the egg against bacterial invasion.

Introduction

Organized macromolecular assembly of protein/polysaccharides regulates mineral formation in biology.[1−3] The ability of a biomacromolecule to self-assemble is one of the most complex and intriguing properties of the soluble organic matrices present in various biomineralized structures.[4,5] Little is known about the way these proteins assemble into a precisely arranged network capable of directing the mineralization.[6] Calcified eggshell is an excellent biomineral model system for investigation.[7] Eggshell is a macroporous respiratory house with multifunctional characteristics for embryonic survival.[8] In both avian and testudine eggshells, $CaCO_3$ is the mineral used for shell construction. At the same time, calcite is the mineral phase found in all avian eggshells, while aragonite is commonly found in a great number of testudine eggshells. Chinese soft-shelled turtles, *Pelodiscus sinensis*, belong to the family Trionychidae and inhabit common waterways. These turtles lay eggs in loose soil or on sandy shores in sunny and sheltered areas. Unlike avian eggshells, the turtle eggshell is pliable due to a less compact arrangement of the mineral phase and does not contain a cuticle layer; therefore, resistance to bacterial penetration is provided by the mineral layer, shell membrane, and albumen.[9] The shell also provides about 60−75% of the calcium that is required for the embryonic development.[10] During the formation of eggshell, mineral deposition is initiated on a discrete fibrous shell membrane, which acts as a nucleation site for further crystal growth (Figure 1A). The cross section of the eggshell after bleach treatment reveals a close-packed arrangement of acicular needles of 2 μm thick aragonite crystals that radiate from the nucleation site (Figure 1B,C). The tip of the shell unit closer to the shell membrane is shown in Figure 1D. We reported earlier the purification and characterization of a 4.2 kDa peptide,

[†] Department of Chemistry, National University of Singapore.
[‡] Department of Biological Sciences, National University of Singapore.
[§] Department of Anatomy, National University of Singapore.
[||] University of Louisiana.

(1) Dauphin, Y. *Zoology* **2006**, *109*, 85−95.
(2) Marin, F.; Pokroy, B.; Luquet, G.; Layrolle, P.; De Groot, K. *Biomaterials* **2007**, *28*, 2368−2377.
(3) Weiner, S.; Dove, P. M. *Rev. Mineral. Geochem.* **2003**, *54*, 1−29.
(4) (a) Fincham, A. G.; Moradian-Oldak, J.; Simmer, J. P. *J. Struct. Biol.* **1999**, *126*, 270−299. (b) De Yoreo, J. J.; Dove, P. M. *Science* **2004**, *306*, 1301−1302.
(5) Weaver, J. C.; Aizenberg, J.; Fantner, G. E.; Kisailus, D.; Woesz, A.; Allen, P.; Fields, K.; Porter, M. J.; Zok, F. W.; Hansma, P. K.; Fratzl, P.; Morse, D. E. *J. Struct. Biol.* **2007**, *158*, 93−106.
(6) Evans, J. S. *Curr. Opin. Colloid Interface Sci.* **2003**, *8*, 48−54.
(7) Heuer, A. H.; Fink, D. J.; Laria, V. J.; Arias, J. L.; Calvert, P. D.; Kendall, K.; Messing, G. L.; Blackwell, J.; Rieke, P. C.; Thompson, D. H.; Wheeler, A. P.; Veis, A.; Caplan, A. I. *Science* **1992**, *255*, 1098−1105.
(8) Nys, Y.; Gautron, J.; Garcia-Ruiz, J. M.; Hincke, M. T. *C. R. Paleval* **2004**, *3*, 549−562.
(9) Solomon, S. E.; Baird, T. *J. Exp. Mar. Biol. Ecol.* **1976**, *22*, 145−160.
(10) Sahoo, G.; Sahoo, R. K.; Mohanty-Hejmadi, P. *Comp. Biochem. Physiol., Part A: Comp. Physiol.* **1998**, *121*, 91−97.

10.1021/ja075659k CCC: $40.75

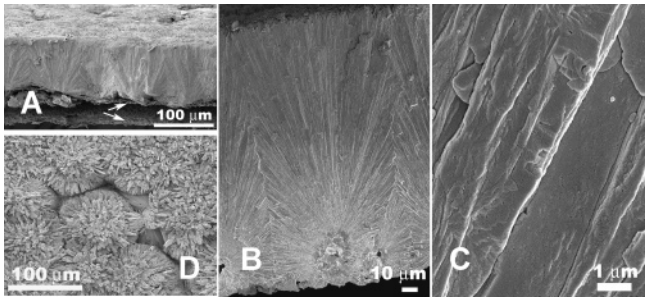

Figure 1. Ultrastructure of turtle eggshell. (A) Cross section of the whole turtle eggshell. The white arrow indicates the shell membrane. (B) Cross section of the bleach-treated eggshell. Note that the membrane is completely removed after bleach treatment. (C) Magnified image of central portion of crystalline layer. (D) Crystalline layer that is attached to the shell membrane. Note the acicular needles of aragonite radiate from the center.

pelovaterin, from the bleach-treated eggshell matrix.[11] Pelovaterin is a glycine-rich peptide containing 42 amino acid residues with three intramolecular disulfide bonds; it is the major intracrystalline component in the eggshell. The amino acid sequence of pelovaterin does not show homology to any known proteins/peptides in the databases; therefore, its function in the eggshell is difficult to predict. Our aim is to gain a better understanding of the role of pelovaterin in the eggshell matrix. In this paper, we determine the 3D (tertiary) solution structure of pelovaterin by two-dimensional (2D) ^{1}H NMR and we investigate its role in antimicrobial and mineral-inducing properties. Owing to its high abundance in the intracrystalline matrix, we have also investigated the self-aggregating (quaternary structure) properties by various biophysical techniques.

Experimental Section

Extraction, Purification, and Characterization of Pelovaterin. Pelovaterin was extracted from bleach-treated eggshells. The white crystalline powder (~10 g) was suspended in 100 mL of Milli-Q water and decalcified by the gradual addition of 2 N HCl overnight at 4 °C under constant stirring. The solution was concentrated on an Amicon microconcentrator (200 mL, YC05 membrane filter, 500 MW cutoff) at 4 °C. After the solution was concentrated to 40 mL, about 150 mL of Milli-Q water was added and the solution was further concentrated. The procedure was repeated 5−6 times to remove the salts; the turbid solution was then centrifuged for 30 min at 3000*g*, and the supernatant was lyophilized. Excess water was added to the residue, the mixture was shaken overnight on a tabletop auto shaker at 4 °C, and the supernatant was lyophilized. The procedure was repeated 3 times to extract the water-soluble intracrystalline organic matrix. The total soluble organic matrix is estimated by weighing the obtained residue from the lyophilization of supernatant liquid. This method produced higher yield than the dialysis method reported earlier.[11] Three independent extractions were performed. The total soluble and insoluble intracrystalline organic matrixes have been found to be 1.74% ± 0.09% (w/w) and 0.42% ± 0.03% (w/w), respectively. The soluble organic matrix (SOM) was dissolved in water/7.5 mM $CaCl_2$, loaded onto a C18 reversed-phase column, and eluted against a linear gradient of 0.1% trifluoroacetic acid in 80% acetonitrile. From 1 mg of the SOM, we obtained about 0.92 ± 0.3 mg of pelovaterin.

NMR Spectroscopy. NMR samples were prepared by dissolving 2.1 mg of pelovaterin in 540 μL of H_2O and 60 μL of D_2O. The pH of the sample was kept at 4.5, and no buffer solution was added to the sample. To determine the optimal conditions for obtaining well-resolved NMR spectra, 2D nuclear Overhauser spectroscopy (NOESY; mixing times of 300, 200, and 150 ms) and total correlation spectroscopy (TOCSY; mixing times of 80 and 120 ms) were employed to acquire spectra at 298, 303, and 308 K on a Bruker Avance 800 MHz NMR spectrometer.[12,13] For a better comparison with the structures of other defensins, we determined the structure of pelovaterin in 90% water/10% D_2O. To examine the effects of calcium, we have recorded six 2D TOCSY spectra with different concentrations of $CaCl_2$ starting from 0, 1.5, 3.5, 5.5, 7.5, and 10 mM with 16 scans and 512 *t*1 increments, and a relaxation delay of 1 s was used for each 2D experiment. There were no significant chemical shift changes in the proton resonances in all the 2D TOCSY spectra with or without $CaCl_2$ (data not shown), indicating no significant change in the structure of pelovaterin in the presence of $CaCl_2$. Complete details of the 3D structure determination by NMR are provided in the Supporting Information.

Antimicrobial Activity. The morphological changes induced by pelovaterin for *P. aeruginosa* and *P. vulgaris* were examined on a Philips XL 30 FEG scanning electron microscope. The sample preparations were made by the method of Motizuki et al.[14] Briefly, pelovaterin (50 μL in 7.5 mM $CaCl_2$) was incubated with a 1 mL suspension of the bacteria (1.0×10^5 colony−forming units (cfu)/mL) for 24 h at 37 °C. An equivalent amount of $CaCl_2$ without pelovaterin served as the negative control. After removal of a small portion of these samples for cfu measurements, the remainder was centrifuged for 10 min at 2800 rpm. Pellets were resuspended and fixed with an equal volume of 5% glutaraldehyde in 1 mM phosphate buffer (pH 7.4) for 1 h. Immediately following the addition of the fixative solution, the sample tubes were mixed by gently inverting the tube up and down for several minutes to prevent clumping of the cells. The cells were postfixed for an additional 1 h with 1% osmium tetroxide (OsO_4) in PBS and washed three times in PBS. The cells were spotted on a sterile cover glass, left to stand for 20−30 min, and then dehydrated by a gradient ethanol wash. The samples were transferred in 100% ethanol to a critical point dryer (Balzers CPD-030, Bal-Tec AG, Vaduz, Liechtenstein), and dried with liquid CO_2 as the transition solvent. The samples were then mounted on an aluminum stub coated with double-sided carbon tape, sputter-coated with gold, and examined.

$CaCO_3$ Crystallization Experiments. $CaCO_3$ crystal growth experiments were performed as previously described.[11] The recrystallization experiment was performed by purging CO_2 to a stirred suspension of biogenic $CaCO_3$ obtained from bleach-treated turtle eggshells for 90 min.[15] The suspension was filtered through 0.45 μm filters and CO_2 was bubbled into the clear solution again for 30 min to dissolve any residual nuclei formed. The pH of the solution was 5.9. About 1 mL of this supersaturated $Ca(HCO_3)_2$ was placed on a 12 mm cover slip kept in a 3 cm petri dish covered with aluminum foil with a few pin holes. The morphology of the $CaCO_3$ crystals formed was examined on a Phillips XL 30 FEG scanning electron microscope at 15/20 kV after they were sputter-coated with gold to increase the conductivity. The mineral phase was identified by use of micro-Raman spectra acquired at room temperature in the backscattering geometry with a single-grating Raman spectrophotometer (Model Spex T64000, Jobin Yvon, France). Powder X-ray diffraction (PXRD) of the mineral phase formed in the recrystallization experiment was performed on a D5005 Siemens X-ray diffractometer with Cu Kα radiation at 40 kV and 40 mA.

Size-Exclusion Chromatography. Self-aggregation of pelovaterin was investigated on a Superdex 75 gel-filtration column attached to an AKTA Purifier system (Amersham Biosciences, Uppsala, Sweden). Pelovaterin (100 μL) was injected into the column pre-equilibrated with 200 mM Tris-HCl containing 7.5 mM $CaCl_2$ (pH = 7.8). $CaCl_2$ solution

(11) Lakshminarayanan, R.; Chi-Jin, E. O.; Loh, X. J.; Kini, R. M.; Valiyaveettil, S. *Biomacromolecules* **2005**, *6*, 1429 − 1437.

(12) Kumar, A.; Ernst, R. R.; Wüthrich, K. *Biochem. Biophys. Res. Commun.* **1980**, *95*, 1−6.
(13) Bax, A.; Davis, D. G. *J. Magn. Reson.* **1985**, *65*, 355−360.
(14) Motizuki, M.; Itoh, T.; Satoh, T.; Yokota, S.; Yamada, M.; Shimamura, S.; Samejima, T.; Tsurugi, K. *Biochem. J.* **1999**, *342*, 215−221.
(15) Lakshminarayanan, R.; Loh, X. J.; Gayathri, S.; Sindhu, S.; Banerjee, Y.; Kini, R. M.; Valiyaveettil, S. *Biomacromolecules* **2006**, *7*, 3202−3209.

(7.5 mM) was used in SEC and other experiments since $CaCl_2$ facilitates the solubility of pelovaterin at high concentrations. The elution of peptides was monitored at 215 nm.

Dynamic and Static Light Scattering Experiments. Dynamic (DLS) and static (SLS) light-scattering measurements were carried out with a BI200SM instrument (Brookhaven Instruments Corp., Holstville, NY). A vertically polarized argon ion laser (514.2 nm and 75 mW) was used as the light source. The particle size and size distribution were obtained by analyzing the field correlation function $|g^{(1)}(\tau)|$ by use of constrained regularized CONTIN program supplied with the instrument. Analytical-grade toluene was used as the calibrating liquid for determining the Rayleigh ratio (R_θ). SLS experiments were performed at scattering angles between 30° and 120° at 5° intervals. The radius of gyration and the molecular mass of the aggregates were estimated by double-reciprocal (Zimm) plot provided with the instrument.

Atomic Force Microscopy. AFM observations were obtained with a Nanoscope IIIA system (Digital Instruments, Santa Barbara, CA) equipped with a vertical-engage *J* scanner. About 50 μL of a dilute solution of pelovaterin in 7.5 mM $CaCl_2$ was spread on a freshly cleaved mica plate for 30 min. The unbound pelovaterin and salts were removed by gentle washing with Milli-Q water. Imaging of the air-dried sample was performed in a tapping mode with standard silicon TESP cantilevers (nominal spring constant 50 N/m; resonance frequency ≈ 270 kHz).

Isothermal Titration Calorimetry. ITC experiments were performed on a VP−ITC titration calorimetric system (Microcal Inc., Northampton, MA). The sample cell had a volume of 1.4 mL and was filled with 7.5 mM $CaCl_2$ solution. A concentrated pelovaterin dissolved in 7.5 mM $CaCl_2$ (8.4 mg/mL) was taken in the 250 μL continuously stirred syringe. Pelovaterin solution (5 μL) was injected into the sample cell at 25 °C with continual stirring at 310 rpm. Each injection was carried out at 300 s intervals to allow the solution to reach equilibrium, and the cell was stirred continuously at 300 rpm. The aggregated pelovaterin in the added solution disintegrates into monomer, which is accompanied by absorption or evolution of heat. As more and more pelovaterin was injected into the cell, the aggregated pelovaterin no longer disintegrates and the heat of disassembly decreases. The midpoint of the transition, the critical aggregation concentration, is obtained by first derivative curve.

Results and Discussion

NMR Data and Structure Calculations. Pelovaterin structure was calculated by use of a total of 597 nonredundant interproton distance constraints and 82 dihedral angle constraints, giving a total of 16 constraints per residue. The NOE distance constraints consisted of 224 intraresidual, 170 sequential, 70 medium-range, and 133 long-range interactions. Structure calculations were performed in an automated manner with CYANA to obtain 50 generated structures. The 20 best structures, considered to be representative of the solution structure of pelovaterin, were used for illustration and statistical analysis (Figure 2A and Table 1). A complete description of the solution structure is provided in the Supporting Information. All the regions of pelovaterin structure are well-defined. The Ramachandran plot exhibits 99.8% of the ϕ, ψ angles of the 20 converged structures in the most favored and additionally allowed regions according to the PROCHECK analysis.[16] An analysis of the ensemble of pelovaterin structures revealed that hydrophilic residues Asp1−Arg7 begin with a random coil structure leading to a short 3_{10} helix between Cys8 and Gly12, whereas antiparallel β-strands are formed by the residues

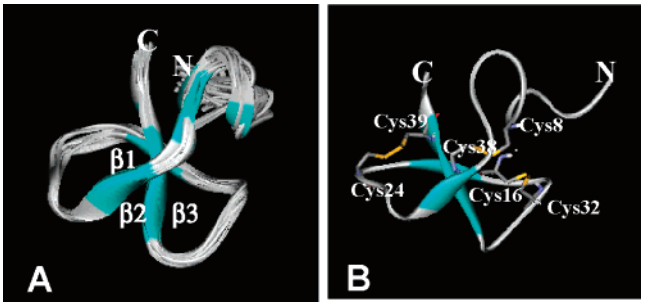

Figure 2. Solution structure of pelovaterin. (A) Best fitted superposition of the 20 structures of pelovaterin. (B) Ribbon diagram of pelovaterin with the three disulfide bonds (shown in gold).

Table 1. Structural Statistics for the Final 20 Models of Pelovaterin

NMR Distance and Dihedral Constraints	
total NOE	597
intraresidue	224
interresidue	
sequential ($\|i-j\|=1$)	170
medium-range ($\|i-j\|<4$)	70
long-range ($\|i-j\|>5$)	133
total dihedral angle restraints	82
Structure Statistics	
violations (mean and SD)	
distance constraints (Å)	<0.2
dihedral angle constraints (deg)	<2
average pairwise rmsd (Å)	
heavy (1−42)	0.83
backbone (1−42)	0.52
Ramachandran Plot Analysis[a] (%)	
most favored region	61.6
additionally allowed region	38.3
generously allowed region	0.2
disallowed region	0.0

[a] PROCHECK.

Leu17−Val20 (β1), His27−Val28 (β2), and Gly34−Cys39 (β3) arranged in a $\alpha\beta_1\beta_2\beta_3$ topology (Figure 2B). Strand β1 is hydrogen-bonded to strand β3, which is in turn hydrogen-bonded to β2. The packing of the helix is constrained by the formation of a disulfide bond between Cys8 and Cys38. The amino acid sequence and NMR structure indicates that pelovaterin has a large central hydrophobic core with a few hydrophilic amino acid residues at the N- and C-termini. Pelovaterin is a glycine-rich peptide (21.4%), enabling the structure to have many turns.

Comparison of Pelovaterin Structure with β-Defensins and β-Defensin-like Peptides. The 3D structure of pelovaterin exhibits significant similarity with cationic antimicrobial peptides derived from mammals, known as defensins (Figure 3).[17,18] The structural similarity is particularly striking due to very low sequence identity of pelovaterin with other defensins. Presumably, a similar arrangement of disulfide linkages rendered pelovaterin to adopt a β-defensin-like fold (Table 2).[19] A number of polypeptides derived from penguin stomach and from venoms of sea anemones, snake, and platypus are shown to adopt a

(16) Laskowski, R. A.; Rullmann, J. A. C.; MacArthur, M. W.; Kaptein, R.; Thornton, J. M. *J. Biomol. NMR* **1996**, *8*, 477−486.
(17) Ganz, T.; Lehrer, R. I. *Pharmacol. Ther.* **1995**, *66*, 191−205.
(18) Kobayashi, Y.; Sato, A.; Takashima, H.; Kyogoku, Y.; Lambert, P.; Kuroda, H.; Chino, N.; Watanabe, T, X.; Kimura, T.; Sakakibara, S.; Moroder, L. *Biopolymers* **1991**, *31*, 1213−1220.
(19) Schibli, D. J.; Hunter, H. N.; Aseyev, V.; Starner, T. D.; Wiencek, J. M.; McCray, P. B.; Tack, B. F.; Vogel, H. J. *J. Biol. Chem.* **2002**, *277*, 8279−8289.

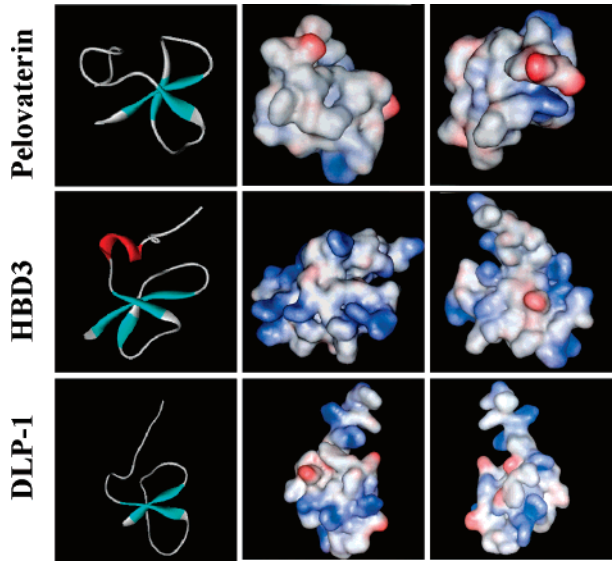

Figure 3. Comparative NMR structure analysis: Comparison of ribbon diagram and electrostatic surface plots of the most representative NMR structures of pelovaterin, human β-defensin 3 (HBD3, ref 19), and defensin-like peptide from platypus venom (DLP1, ref 23). The center panel indicates surface plot in the same orientation as in ribbon diagram while in the last panel, the structures are rotated 180° around the *y*-axis. The blue shade in the surface structure represents the positively charged domain, while the red shade represents negatively charged domain.

β-defensin-like fold.[20−23] This is the first report of a peptide with β-defensin-like fold from a biomineralized tissue. Sequence comparison reveals the conservation of residues responsible for the formation of the β-defensin fold, including six cysteine residues, Gly12, and Gly31. Another notable conserved domain in pelovaterin and β-defensins is the presence of a −CCX- motif (where X = R or K) at the C-terminus. The rest of the residues are completely nonconserved in pelovaterin. All cysteine residues are found to be topologically equivalent and disulfide-bonded in an identical fashion in these peptides. Similar to other defensins and defensin-like peptides, the C-terminal β-strand in pelovaterin is sandwiched between two antiparallel β-strands. Despite the overwhelming similarity in the tertiary fold, there are significant differences in the fine structure of pelovaterin, suggesting different biological functions and divergent evolution. The most obvious of these is the net charge of the molecule. There are three negatively and two positively charged residues in pelovaterin, giving an overall net charge of −1, whereas defensins are largely cationic in nature (Table 2). There are significant differences in the location and distribution of the positive charges among these three peptides. In pelovaterin, the N- and C-terminal arginine residues are positioned on opposite faces, whereas in defensin-like peptide from platypus venom (DLP-1) and in human β-defensin 3 (HBD3), the cationic residues are distributed throughout the surface randomly.

Antimicrobial Activity of Pelovaterin. Defensins exhibit antimicrobial activity against a number of pathogens, including bacteria and fungi. Because of its topological similarity, the antimicrobial activity of pelovaterin against five Gram-negative and one Gram-positive bacteria was investigated by disc diffusion and Mueller−Hinton broth dilution methods (see Supporting Information). Pelovaterin exhibited strong antimicrobial activity against two Gram-negative bacteria, namely, *Pseudomonas aeruginosa* (expressed as effective concentration of pelovaterin required to kill 50% of bacteria, EC_{50} = 0.42 μg/mL) and *Proteus vulgaris* (EC_{50} = 0.37 μg/mL), moderate activity against *Proteus mirabilis* (EC_{50} = 8.4 μg/mL) and *Staphylococcus aureus* (EC_{50} = 42 μg/mL), and poor activity against *Escherichia coli* and *Enterobacter aerogenes*. The activity was not altered significantly in the presence of 7.5 mM $CaCl_2$. The EC_{50} values of pelovaterin against *P. aeruginosa* and *S. aureus* are compared with other defensins and defensin-like peptides (Table 2). The anti *P. aeruginosa* activity of pelovaterin is similar whereas the anti *S. aureus* activity is weaker compared to HBD series of peptides and SPHE2. To study the mechanism of action and structural evidence for the membrane changes in *P. aeruginosa* and *P. vulgaris* induced by pelovaterin, cell imaging was done with a scanning electron microscope. Untreated *P. aeruginosa* and *P. vulgaris* bacterial cells had a smooth texture (Figure 4A,C), but treatment with 10 μM pelovaterin produced pronounced wrinkling, surface roughening, and blebbing of the membrane and the majority of the cells lost their membrane integrity (Figure 4B,D). The appearance of cellular debris suggests possible leakage and cell lysis. Although not fully understood, the mechanism of bactericidal action of the defensins depends on noncovalent interactions between the defensins and the cell membrane.[24] The defensins bind to the bacterial membrane through electrostatic interaction, and a homodimer is formed when defensins enter through the cell membrane. The dimer is formed in such a way that a hydrophobic interface attaches to the inner membrane, while hydrophilic sites face each of the β-defensin monomers and disrupts the membrane permeability by altering the transmembrane potential, which then leads to cell death. Thus the total net charge and the overall hydrophobicity of defensins are crucial for antimicrobial activity. The overall hydrophobicity of a peptide at the membrane interface (measured as ΔG) is calculated by the Wimley and White hydrophobicity scale.[25] The free energy contribution of all naturally occurring amino acid residues in transferring a peptide from a bilayer interface to water is presented in this scale. A positive ΔG indicates a hydrophobic peptide. Figure 5 shows the sum of hydrophobicity values of the constituent amino acid residues, ignoring the structural details. The antimicrobial active and inactive peptides are clearly represented by two different regions. DLP1−3 are the defensin-like peptides from platypus venom that do not have any antimicrobial properties. It is interesting to note that the most potent antimicrobial peptides HBD3 and SPHE2 occupy extreme positions, highlighting the importance of both hydrophobicity and net charge in the potent antimicrobial properties. Clearly, pelovaterin occupies a different position although its hydrophobicity is comparable to that of SPHE1/2 (Figure 5). Therefore, factors such as strong resemblance with the β-defensin fold, including the conservation of some key structural residues, the arrangement of disulfide bridges, and overall

(20) Landon, C.; Thouzeau, C.; Labbe, H.; Bulet, P.; Vovelle, F. *J. Biol. Chem.* **2004**, *279*, 30433−30439.
(21) Fogh, R. H.; Kem, W. R.; Norton, R. S. *J. Biol. Chem.* **1990**, *265*, 13016−13028.
(22) Nicastro, G.; Franzoni, L.; de Chiara, C.; Mancin, A. C.; Giglio, J. R.; Spisni, A. *Eur. J. Biochem.* **2003**, *270*, 1969−1979.
(23) Torres, A. M.; Wang, X. H.; Fletcher, J. I.; Alewood, D.; Alewood, P. F.; Smith, R.; Simpson, R. J.; Nicholson, G. M.; Sutherland, S. K.; Gallagher, C. H.; King, G. F.; Kuchel, P. W. *Biochem. J.* **1999**, *341*, 785−794.
(24) Sugiarto, H.; Yu, P. L. *Biochem. Biophys. Res. Commun.* **2004**, *323*, 721−727.
(25) Wimley, W. C.; White, S. H. *Nat. Struct. Biol.* **1996**, *3*, 842−848.

Table 2. Comparison of the Amino Acid Sequence and Antimicrobial Properties of Pelovaterin with Other β-Defensins and Defensin-like Peptides

Peptide	Amino acid sequence	Disulphide pattern	Net Charge	[a]ΔG, kCal/mole	[b]EC_{50} µg/mL	
					G^+	G^-
Pelovaterin	DDTPSSRCGSG-GWGPCLPIVDLLCIVHVTV-G-CS-GGFGCCRIG	$CX_7CX_7CX_7CX_5CCX_3$	-1	-0.97	42.5	0.42
HBD1	GLGHRSDHYNCVSS-GGQ-CLYSA---CPIFTKIQGTCYRGKAKCCK	$CX_6CX_4CX_9CX_6CCX_1$	+4/+5	-2.75	weak[c]	1.5[c]
HBD2	GIGDPVTCLKS-GAI-CHPVF---CPRRYKQIGTCGLPGTKCCKKP	$CX_6CX_4CX_9CX_6CCX_3$	+6	-6.16	>100	0.12[c]
HBD3	GIINTLQKYYCRVR-GGR-CAVLS---CLPKEEQIGKCSTRGRKCCRRKK	$CX_6CX_4CX_9CX_6CCX_4$	+11	-12.65	5-10[d]	5-10[d]
DLP1	FVQHRPRDCESINGV--CRHKDTVNCREIFL--ADCYNDGQKCCRK	$CX_6CX_7CX_7CX_6CCX_2$	+2	-14.04	-	N.A.[e]
SPHE2	SFGLCRLRRGF--CARGR---CRFPSIPIGRCS-RFVQCCRRVW	$CX_6CX_8CX_8CX_5CCX_4$	+10	-0.77	<6.8[f]	<27[f]

[a] Calculated from Ref. 25. [b] Indicates the effective concentration of peptide required to kill 50% of the bacteria. The values are reported for *S. aureus* (G^+) and *P. aeruginosa* (G^-) only. [c] Obtained from Ref.52. [d] Taken from Ref.53. [e] Indicates no activity. [f] The minimum inhibitory concentration values are taken from Ref.54.'-' indicates not known. The disulfide bonded cysteines in pelovaterin are colored identically. The red and blue colored letters indicate negative and positive charged amino acid residues, respectively.

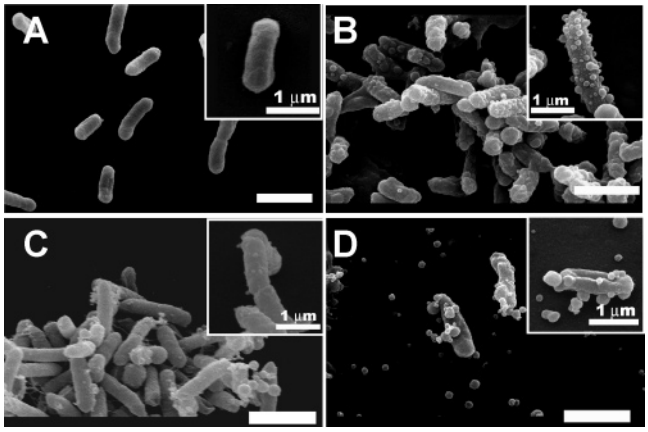

Figure 4. Antimicrobial activity of pelovaterin: electron micrographs of *P. aeruginosa* incubated (A) without and (B) with 10 μM pelovaterin And of *P. vulgaris* incubated (C) without and (D) with 10 μM pelovaterin. Scale bar = 2 μm.

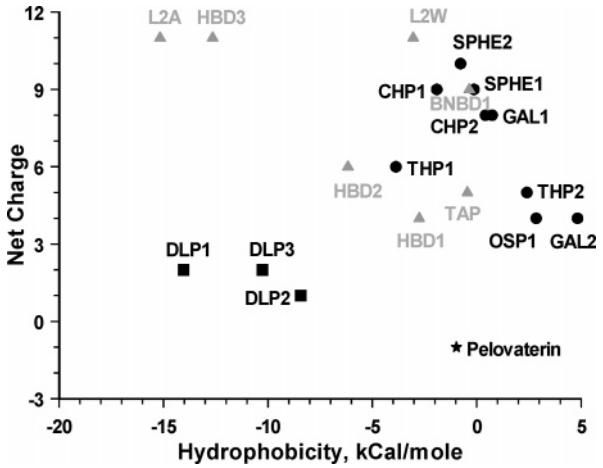

Figure 5. Correlation of the net charge and the Wimley and White hydrophobicity score of pelovaterin and β-defensin-like proteins. HBD1−3 are human β-defensin peptides. L2A and L2W are the 40 amino acid residues of the HBD3 derived peptides that lack five residues at the N-terminus and in which six cysteine residues were replaced by alanine or tryptophan.[55] TAP and BNBD1 are β-defensins from bovine trachea and neutrophil. DLP1−3 are β-defensin-like peptides from platypus venom. SPHE1,2 are β-defensin-like peptides from penguin stomach. CHP1,2 and GAL1,2 are β-defensin-like peptides isolated from heterophils of chicken. THP1,2 and OSP1 are β-defensin-like peptides isolated from heterophils of turkey and ostrich, respectively.

hydrophobicity, might explain the common tendency to interact with lipid membranes and the antimicrobial activity of pelovaterin.

Interaction of Pelovaterin with $CaCO_3$. To understand the role of pelovaterin in eggshell formation, we performed in vitro crystallization experiments at various concentrations. The morphology of $CaCO_3$ crystals changes significantly with the concentration of pelovaterin. A mixture of vaterite and calcite crystals was observed upon introduction of 50 ng/mL pelovaterin into the crystallization milieu.[11] Increasing the concentration of pelovaterin (5 and 50 μg/mL) resulted in the formation of large floret-shaped crystals (Figure 6A,B); and at higher concentrations of pelovaterin (5 and 8 mg/mL), a mineral film with intermittent cracks was formed (Figure 6C,D). These mineral films consist of an assemblage of fused smaller spherical vaterite particles. However, in the control experiment (i.e., without pelovaterin), regular rhombohedral calcite crystals were formed (Figure 6E). The mineralogy of the particles was investigated by Fourier transform (FT)-Raman spectroscopy. The presence of a splitting in the ν_1 absorption band of carbonate at 1090 cm^{-1} indicates the presence of vaterite phase (Figure 7A,B). Calcite and aragonite do not have this splitting and the latter two can be distinguished by the appearance of splitting in the ν_4 absorption band for aragonite (Figure 7C,D). It has been demonstrated that macromolecules extracted from mollusk shells induced aragonite formation only if they were assembled on a chitin−silk fibroin complex, indicating the requirement for an appropriate microenvironment for aragonite nucleation.[26] Since eggshell calcification takes place on regiospecific sites on a highly hydrophobic shell membrane, crystallization experiments were performed by adsorbing pelovaterin on decalcified eggshell membrane (Supporting Information). Even under these conditions, vaterite was the major polymorph, indicating that crystallization conditions did not mimic the biological environment. Hence, we performed recrystallization experiments using a modified Kitano's method.[15] Under these conditions, acicular needles were formed along with minor amount of rhombohedral

(26) Falini, G.; Albeck, S.; Weiner, S.; Addadi, L. *Science* **1996**, *271*, 67−69.

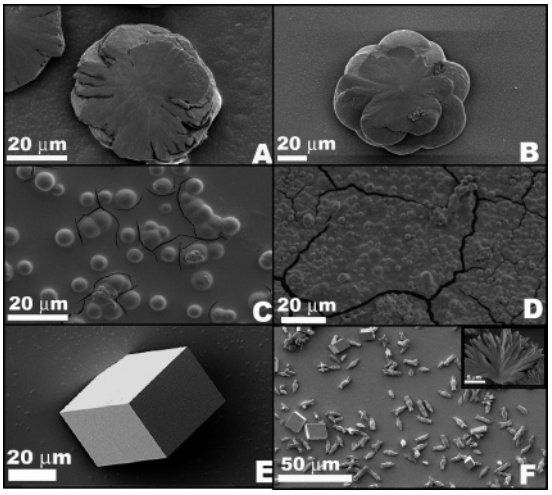

Figure 6. Effect of pelovaterin on $CaCO_3$ crystallization. Representative electron micrographs are shown of $caCO_3$ grown in the presence of pelovaterin at different concentrations: (A) 5 μg/mL; (B) 50 μg/mL; (C) 5 mg/mL; (D) 8 mg/mL; (E) control (no pelovaterin). (F) Aragonite crystals obtained from recrystallization experiments.

calcite crystals (Figure 6F). Powder XRD of the crystals confirmed the presence of aragonite as the dominant polymorph (Figure 7E). The amount of aragonite phase is estimated to be 86% ± 3%, based on the method reported by Kontoyannis and Vagenas.[27] Since pelovaterin is the major intracrystalline peptide isolated from turtle eggshells, the recrystallization experiment suggests that pelovaterin has the ability to induce and stabilize metastable polymorphs.

Evidence for Micellar Self-Assembly. The transformation of vateritic single crystal to thin film with increasing concentration indicates significant changes in the solution behavior of pelovaterin. To obtain better insight into these changes, SEC, laser light scattering, and AFM experiments were performed. At high concentration (8 mg/mL), pelovaterin elutes at ~9.5 mL on a Superdex 75 column, earlier than expected for a 4.2 kDa peptide (Figure 8A). At lower concentrations (2 mg/mL), it elutes around 14 mL and the ~9.5 mL peak disappears. These results are consistent with polymeric aggregates being the predominant form of pelovaterin at higher concentrations. The physical status of pelovaterin aggregates in solution was also established by static and dynamic light scattering experiments. At 8 mg/mL, the result showed a single scattering population of hydrodynamic diameter (D_h) 52 nm (Figure 8B). Such a large size is unusual for a peptide with 42 amino acid residues and indicates the existence of "polymeric" forms of pelovaterin.[28] To estimate the average molecular mass of the aggregates and the aggregation number, static light scattering (SLS) experiments were performed (Figure 8C). SLS data, analyzed through a Zimm plot, indicate a radius of gyration (R_g) of 31.1 ± 1.2 nm. The ratio R_g/R_h is characteristic of the structure of scattering particles in solution and is 0.77, 1.78, and >2 for a solid spheres, random coils, and rodlike structures, respectively. A value of 1.2 indicates that pelovaterin aggregates are not solid spheres but behave like vesicular hollow spheres.[29] The mass of the aggregates (M_w) determined from the Zimm plot is 215 000 ± 27 000 g/mol, indicating that the aggregates contain ~51 ± 7 pelovaterin monomers and accounting for the early exclusion in SEC and large particle size observed in the DLS measurements. Since a rigid sphere with a size of 52 nm contains about 8000 monomers, the estimated low aggregation number may further point to a hollow interior of the nanospheres. A negative value obtained for the second virial coefficient ($A_2 = -1.12 \times 10^{-4} \pm 3.7 \times 10^{-5}$ cm^3 mol g^{-2}) from the slope of the curve suggests the presence of weak attractive intermolecular interactions between pelovaterin aggregates.[30] The morphology of the aggregates was investigated by AFM, which detected the presence of regular spherical particles throughout the mica surface (Figure 8D). The calculated diameters of about 500 particles suggest that the size distribution is fairly homogeneous and large (42 ± 3.0 nm), which is about 10 ± 3 nm less than the hydrodynamic diameter observed by DLS. The disagreement between DLS and AFM is due to the fact that the former measures hydrodynamic diameter while the latter measures diameter of the collapsed dry aggregates. Such a discrepancy has been observed for micelles formed by polymeric and organometallic micelles.[31] In addition to the nanospheres, a small number of protofibrils were also seen (Figure 8D, white arrows). The length of these protofibrils varied from 500 nm to 1.3 μm. The aggregation of pelovaterin to nanospheres and presence of linear assemblies reminiscent of protofibrillar species were similar to the ones observed for the amyloid-forming Aβ peptides.[32] The SLS and AFM results indicate that the nanospheres resemble surfactant micellar assemblies.

Energetics of Pelovaterin Self-Assembly. We performed ITC−dilution experiments to determine the thermodynamic driving force for aggregation of pelovaterin.[33] About 50 injections of 5-μL aliquots of a concentrated solution (8.4 mg/mL) of pelovaterin in 7.5 mM $CaCl_2$ were added to the sample cell containing 7.5 mM $CaCl_2$. Each injection produced heat flow, and the total heat of the reaction was obtained by integration of the peaks (Figure 8E). At 25 °C, exothermic heat was observed for all injections. The integration of the power peaks and normalization by the injected mole number gives the molar heat of demicellization (Figure 8F). The enthalpogram can be divided into two regions where reaction enthalpies remain constant (first injection and final few injections) and the intermediate region, where reaction enthalpies change drastically. Dissociation of the aggregates (disaggregation) and dilution of the monomer may contribute to the large heat changes observed in the first injection. As more pelovaterin was injected into the sample cell, the concentration increases and reaction enthalpy decreases (intermediate region) and at the final concentrations that are well above the critical aggregation concentration (cac), the reaction enthalpy remains essentially constant. Further addition of pelovaterin above the cac does not disintegrate the micelles, and the residual heat observed is due to dilution of aggregates. The difference in enthalpy of the two plateaus gives the enthalpy of demicellization (ΔH_{demic}). The enthalpy of micellization ΔH_{mic}, which has same magnitude as

(27) Kontoyannis, C. G.; Vagenas, N. V. *Analyst* **2000**, *125*, 251−255.
(28) Wilkins, D. K.; Grimshaw, S. B.; Receveur, V.; Dobson, C. M.; Jones, J. A.; Smith, L. J. *Biochemistry* **1999**, *38*, 16424−16431.
(29) Liu, T. B.; Diemann, E.; Li, H. L.; Dress, A. W. M.; Muller, A. *Nature* **2003**, *426*, 59−62.
(30) Narayanan, J.; Liu, X. Y. *Biophys. J.* **2003**, *84*, 523−532.
(31) (a) Gohy, J. F.; Hofmeier, H.; Alexeev, A.; Schubert, U. S. *Macromol. Chem. Phys.* **2003**, *204*, 1524−1530. (b) Dominguez-Gutierrez, D.; Surtchev, M.; Eiser, E.; Elsevier, C. J. *Nano Lett.* **2006**, *6*, 145−147.
(32) Kowalewski, T.; Holtzman, D. M. *Proc. Natl. Acad. Sci. U.S.A.* **1999**, *96*, 3688−3693.
(33) Paula, S.; Sus, W.; Tuchtenhagen, J.; Blume, A. *J. Phys. Chem.* **1995**, *99*, 11742−11751.

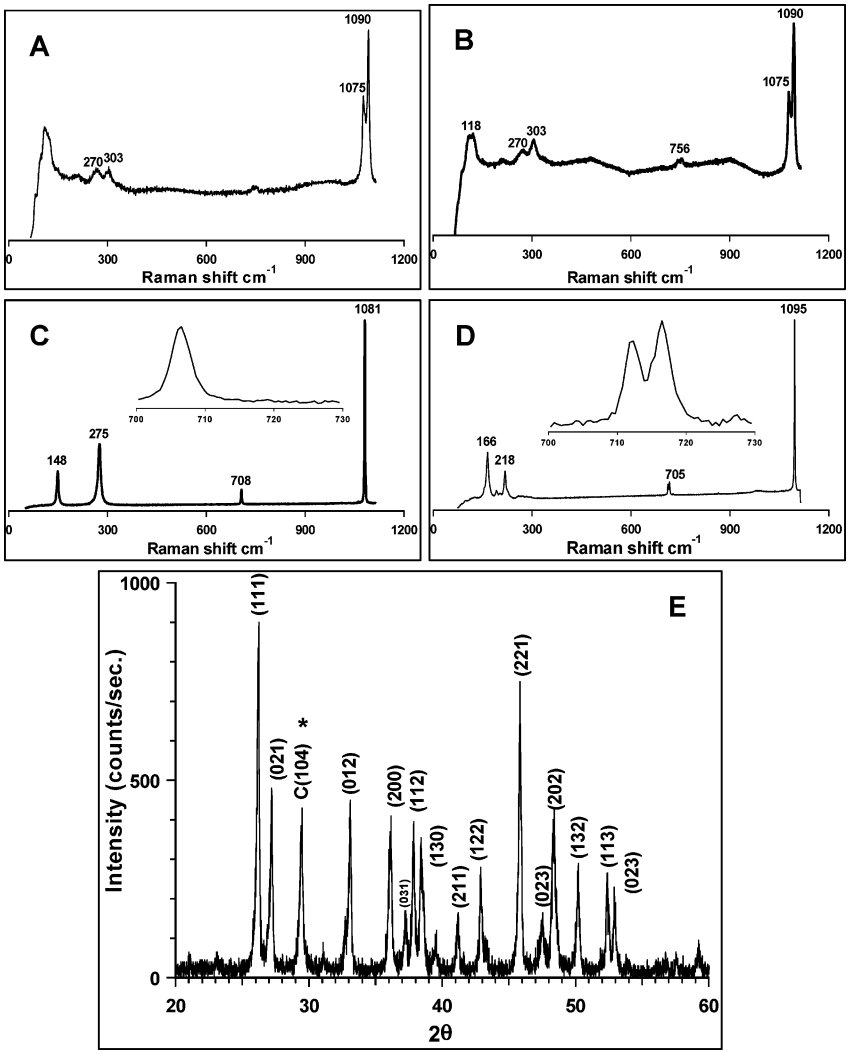

Figure 7. Characterization of the mineral phase: FT-Raman spectroscopy of the mineral phase formed in the presence of pelovaterin at (A) 5 mg/mL and (B) 8 mg/mL. For comparison, FT-Raman spectra of the calcite crystals (C) obtained in the control experiment and of biogenic aragonite (D) are also shown. The ν_4 absorption bands of calcite and aragonite are expanded for clarity. (E) Powder XRD of the mineral phase formed in the recrystallization experiments with all aragonite peaks indexed. (104) of calcite phase is indicated by asterisks.

ΔH_{demic} but opposite sign, was obtained from equation reported by Heerklotz et al.[34]

As the net charge on pelovaterin monomer is −1 and the ITC dilution experiment is carried out in 7.5 mM $CaCl_2$, it is conceivable to have an ionic detergent-like model for pelovaterin. The Gibbs free energy of micellization (ΔG_{mic}) of an ionic detergent is related to the cac by $\Delta G_{mic} = (1+\beta)RT \ln [(cac)/C_w]$, where R is the gas constant, T is the absolute temperature, β is the counterion condensation ($\beta = m/n$, where m is the number of counterions bound per micelle and n is the aggregation number of a micelle), and C_w (=55.5 M) denotes the concentration of water. The cac, determined from the midpoint of the titration, is 134 μM. By use of a known aggregation number and the equilibrium constant, β (=0.16 ± 0.03), ΔG_{mic} was determined.[35,36] From ΔG_{mic}, value of the ΔS_{mic} was calculated from $\Delta G_{mic} = \Delta H_{mic} - T\Delta S_{mic}$. The results indicated that micellization of pelovaterin is a thermodynamically allowed process ($\Delta G_{mic} = -8.9$ kcal/mol), and driven by favorable entropy ($\Delta S_{mic} = +36.5$ cal/mol·K) and unfavorable enthalpy ($\Delta H_{mic} = +1.98$ kcal/mol) changes.

Possible Role of Pelovaterin in the Eggshell. Eggshell is a sophisticated chemical defense against mechanical stress and microbial invasion for embryonic development. Any form of defect or damage of the shell causes microbial infection, results in embryonic mortality, and has important economic implications for the poultry industry. The matrix proteins are distributed throughout the eggshells in small amounts and they could act as excellent chemical defenses against microbes. This mechanism has been documented in vitro for the avian eggs.[37] It is not surprising, because the antimicrobial properties of egg white proteins such as lysozyme and ovotransferrin, which are components of the avian eggshell extract, are well-known.[38,39] In turtle eggshells, pelovaterin is the major component and neither lysozyme nor ovotransferrin was detected.[11] To understand the structure−function relationship of pelovaterin in the

(34) Heerklotz, H.; Tsamaloukas, A.; Kita-Tokarczyk, K.; Stunz, P.; Gutberlet, T. *J. Am. Chem. Soc.* **2004**, *126*, 16544−16552.
(35) Beyer, K.; Leine, D.; Blume, A. *Colloids Surf., B* **2006**, *49*, 31−39.
(36) Garidel, P.; Hildebrand, R.; Neubert, R.; Blume, A. *Langmuir* **2000**, *16*, 5267−5275.
(37) Mine, Y.; Oberle, C.; Kassify, Z. *J. Agric. Food. Chem.* **2003**, *51*, 249−253.
(38) Lesnierowski, G.; Cegielska-Radziejewska, R.; Kijowski, J. *World Poult. Sci. J.* **2004**, *60*, 303−309.
(39) Valenti, P.; Antonini, G.; Von Hunolstein, C.; Visca, P.; Orsi, N.; Antonini, E. *Int. J. Tissue. Res.* **1983**, *1*, 97−105.

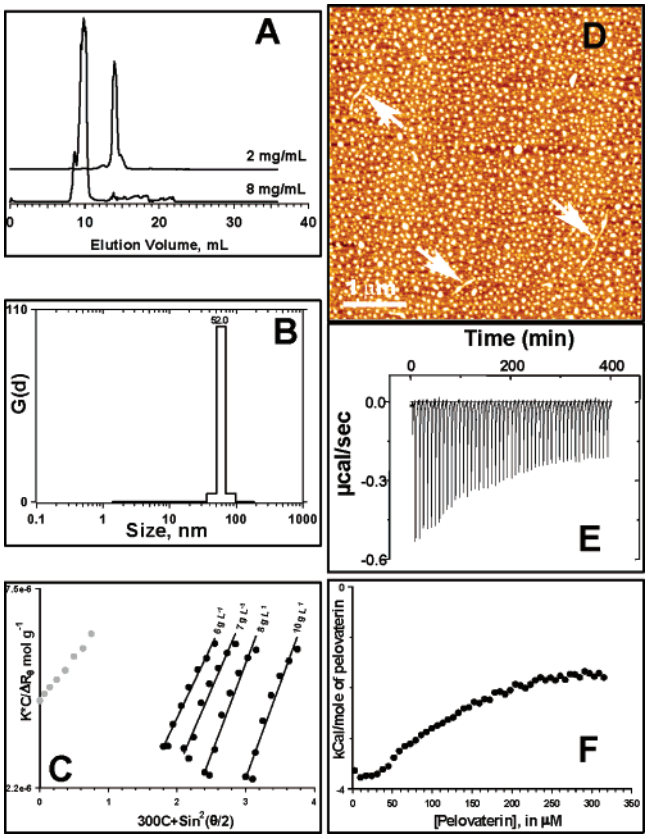

Figure 8. Aggregation properties of pelovaterin. (A) Size-exclusion chromatography of pelovaterin at two different concentrations. (B) CONTIN analysis of DLS measurements on 8 mg/mL pelovaterin solution at 90° scattering angle and (C) Zimm plot of pelovaterin at four different concentrations in 7.5 mM $CaCl_2$. (D) Tapping-mode height image of pelovaterin nanospheres formed after incubation for 30 min. White arrows show the presence of protofibrils. (E) Calorimetric traces (raw data) obtained by titration of a concentrated solution of pelovaterin into 1.4 mL of 7.5 mM $CaCl_2$ solution. (F) Plot of reaction enthalpy per mole of pelovaterin injected versus total concentration of pelovaterin in the cell.

eggshell matrix, its 3D structure was determined. It displays all characteristics of mammalian β-defensins including the presence of a triple-stranded antiparallel β-sheet as the main secondary structural element, the common array of disulfide bonds, and a small helical turn that includes the first cysteine residue. The important features observed in the 3D structure of pelovaterin are the presence of a hydrophobic core and the electrostatic properties of the molecule. A dominant portion of the central core in pelovaterin is hydrophobic in contrast to the hydrophilic defensins and defensin-like peptides. Although, defensins and defensin-like peptides are predominantly cationic, pelovaterin is surprisingly anionic with a net charge of -1. The differences in the hydrophobic and electrostatic properties of these molecules are likely responsible for the differences observed in the activity and solution behavior. Unlike β-defensins, pelovaterin does not exhibit a broad spectrum of antimicrobial activity. Of the six bacterial species examined, only the growth of *P. aeruginosa* and *P. vulgaris* were strongly inhibited. The collapsed morphology of *P. aeruginosa* and *P. vulgaris* as well as the membrane debris is consistent with bactericidal activity of pelovaterin. The EC_{50} of pelovaterin on *P. aeruginosa* is comparable to those of human β-defensins 2/3 and SPHE2. On the basis of the comparable hydrophobicity values, it is conceivable that the anti-*P. aeruginosa* activity of pelovaterin could be through hydrophobic interactions with the membrane. Thus, our results describe a novel chemical defense mechanism acquired by turtle eggshell against the invading microorganisms.

In vitro crystallization experiments demonstrated that pelovaterin induces and stabilizes the metastable vaterite phase. The morphology of vaterite phase also changed significantly with the concentration of pelovaterin, indicating the influence of pelovaterin on the growth process. Aragonite, the mineral phase present in eggshell, is a high-temperature polymorph and its precipitation under ambient conditions requires significantly high amounts of Mg^{2+} in the crystallization milieu.[40] Recrystallization experiments were performed with bleach-treated eggshell matrix dissolved in water, which contains all the matrix components involved in the shell formation. Aragonite was the major polymorph precipitated under these conditions. Elemental analysis of the supersaturated bicarbonate solution showed that the amount of Mg^{2+} (10^{-3} mol % with respect to calcium) is very low to induce any significant amount of aragonite nucleation. Pelovaterin is the major intracrystalline component in turtle eggshell extract, accounting for ~92% of the soluble organic matrix, and it plays an important role in polymorph discrimination as well.

SEC and DLS studies indicated that pelovaterin forms a large protomer assembly at high concentrations. The appearance of nanospheres, high aggregation numbers, and negative ΔG_{mic} values strengthen the micellar geometry of pelovaterin in the aggregated state. The driving force for the micellar aggregation is entropically driven (positive ΔS_{mic} values). The positive ΔS_{mic} can be explained by a classical hydrophobic effect, wherein the insertion of nonpolar molecules is assumed to cause an ordering of water molecules around a nonpolar moiety. Since pelovaterin interfaces are predominantly hydrophobic, there may be considerable numbers of ordered water molecules released upon micellization. The large positive (endothermic) enthalpy change confirms considerable removal of ordered water molecule from the first hydration shell of the hydrophobic residues and may alter the interfacial tension.[41,42] It has been shown that the anionic antibiotic peptide surfactin acts on the interface and core of the membranes mediated by hydrophobic effects, in contrast to the positively charged peptides that have strong influence on the head group structure of the membrane.[43] An elegant demonstration of the role of individual amino acid residues (26 single-site mutants) on the anti-*E. coli* activity has been reported for HBD1 peptides.[44] The results indicated that charged residues alone do not play an important role in the anti-*E. coli* activity. The replacement of N-terminal neutral residues (Y, N, V, and S) also resulted in complete loss or poor anti-*E. coli* activity. Antcheva et al.[45] have shown that removal of an N-terminal aspartic acid (D^4) in human HBD2 resulted in 4−8-fold reduction in anti-*P. aeruginosa* and anti-*S. aureus* activity and suggested that this Asp residue may provide conformational stability that affects the antimicrobial activity. It is possible to

(40) Kitano, Y. *Bull. Chem. Soc. Jpn.* **1962**, *35*, 1973−1980.
(41) Luke, K.; Apiyo, D.; Wittung-Stafshede, P. *Biophys. J.* **2005**, *89*, 3332−3336.
(42) Heerklotz, H.; Seelig, J. *Biophys. J.* **2001**, *81*, 1547−1554.
(43) Heerklotz, H.; Seelig, J. *Biophys. J.* **2000**, *78*, 2435−3440.
(44) Pazgier, M.; Prahl, M.; Hoover, D. M.; Lubkowski, J. *J. Biol. Chem.* **2007**, *282*, 1819−1829.
(45) Antcheva, N.; Boniotto, M.; Zelezetsky, I.; Pacor, S.; Verga, Falzacappa, M. V.; Crovella, S.; Tossi, A. *Antimicrob. Agents Chemother.* **2004**, *48*, 685−688.

have the charged side chains of pelovaterin interacting with water and nonpolar residues reaching into the hydrophobic core of the membrane, which then contribute to destabilization of the membrane.

On the basis of the hydrophobicity plot, it is suggested that the short N-terminal segment and the hydrophobic bulk produce anionic surfactantlike behavior for pelovaterin. The two aspartic acid residues at the N-terminus provide mineral binding potential owing to their flexible location. As the concentration of pelovaterin is increased, the micellar assembly of pelovaterin provides a number of nucleating sites and the molecular mobility is restricted in the aggregated state compared to a monomeric state (from the computed β, we estimated about 8 calcium ions bound per aggregate). Mineral particles continue to grow from each nucleating site until they collide with the neighboring particles resulting in the precipitation of spherical particles that coarsened (due to the presence of rigid template) to form a mineral film.

Since calcite, aragonite, and vaterite differ in interfacial energy by only 4−5 kJ/mol, the order of thermodynamic stability can be inverted by a number of factors.[46,47] Such interfacial recognition of a metastable phase is observed in the in vitro syntheses of $CaCO_3$ polymorphs by polyamide fibers and water-soluble hydrophilic block copolymers and of gallium oxide by the protein filaments present in marine sponge.[48] Thus a surfactantlike assembly of pelovaterin is expected to play an important role in controlling the polymorphism by altering the interfacial energy and formation of mineral coating in vivo. Similar behavior has been reported for the abalone nacre protein in accelerating calcite kinetics.[49]

Conclusion

This study demonstrates the significance of tertiary and quaternary structure of eggshell matrix proteins to perform key tasks that are important for embryonic survival. Tertiary structure of pelovaterin was established by NMR spectroscopy. The β-defensin-like fold and amphiphilic geometry endow pelovaterin with antimicrobial and mineral-modulating properties. Both properties were described with full details. The fundamental construction principles underlying the biological synthesis of inorganic minerals have been thought to provide exciting possibilities for smart materials synthesis.[50] Our work offers an insight into the understanding of multifunctional characteristics of eggshell proteins and provides a new model for the synthesis of structure-based drug design and fabrication of multifunctional materials.[51]

Acknowledgment. R.L. thanks the Singapore Millennium Foundation for the award of fellowship. S.V. thanks the Agency for Science, Technology and Research (ASTAR) and the National University of Singapore for funding support. Technical support from the Departments of Chemistry and Biological Sciences at National University of Singapore is also greatly appreciated.

Supporting Information Available: Detailed NMR structure and statistics, antimicrobial activity by Mueller−Hinton broth dilution method, Raman spectra and electron micrographs of the $CaCO_3$ crystals grown in the presence of pelovaterin on the eggshell membrane, and size-exclusion chromatography. This information is available free of charge via the Internet at http://pubs.acs.org.

JA075659K

(46) Navrotsky, A. *Proc. Natl. Acad. Sci. U.S.A.* **2004**, *101*, 12096−12101.
(47) Colfen, H. *Curr. Opin. Colloid Interface Sci.* **2003**, *8*, 23−31.
(48) (a) Lakshminarayanan, R.; Valiyaveettil, S.; Loy, G. L. *Cryst. Growth Des.* **2003**, *3*, 953−958. (b) Rudloff, J.; Colfen, H. *Lagmuir* **2004**, *20*, 991−996. (c) Kisailus, D.; Choi, J. H.; Weaver, J. C.; Yang, W. J.; Morse, D. E. *Adv. Mater.* **2005**, *17*, 314−318.
(49) Fu, G.; Qiu, S. R.; Orme, C. A.; Morse, D. E.; De Yoreo, J. J. *Adv. Mater.* **2005**, *17*, 2678−2681.
(50) Stupp, S. I. *MRS Bull.* **2005**, *30*, 546−553.
(51) Bellantone, M.; Williams, H. D.; Hench, L. L. *Antimicrob. Agents Chemother.* **2002**, *46*, 1940−1945.
(52) (a) Singh, P. K.; Jia, H. P.; Wiles, K.; Hesselberth, J.; Liu, L.; Conway, B. D.; Greenberg, E. P.; Valore, E. V.; Welsh, M. J.; Ganz, T.; Tack, B. F.; McCray, P. B. *Proc. Natl. Acad. Sci. U.S.A.* **1998**, *95*, 14961−14966. (b) Harder, J.; Bartels, J.; Christophers, E.; Schroder, J. M. *Nature* **1997**, *387*, 861.
(53) Harder, J.; Bartels, J.; Christophers, E.; Schroder, J.-M. *J. Biol. Chem.* **2001**, *276*, 5707−5713.
(54) Thouzeau, C.; Maho, Y. L.; Froget, G.; Sabatier, L.; Bohec, C. L.; Hoffmann, J. A.; Bulet, P. *J. Biol. Chem.* **2003**, *278*, 51053−51058.
(55) Kluver, E.; Schulz-Maronde, S.; Scheid, S.; Meyer, B.; Forssmann, W.-G.; Aldermann, K. *Biochemistry* **2005**, *44*, 9804−9816.